Applied Catalysis B: Environmental 110 (2011) 207–215

Contents lists available at SciVerse ScienceDirect

Applied Catalysis B: Environmental

journal homepage: www.elsevier.com/locate/apcatb

Enhancing the photoelectrochemical performance of hematite (α-Fe_2O_3) electrodes by cadmium incorporation

Ayoung Bak[a], Wonyong Choi[b], Hyunwong Park[a,*]

[a] School of Energy Engineering, Kyungpook National University, Daegu 702-701, Republic of Korea
[b] School of Environmental Science and Engineering, Pohang University of Science and Technology, Pohang 790-784, Republic of Korea

ARTICLE INFO

Article history:
Received 29 June 2011
Received in revised form 19 August 2011
Accepted 7 September 2011
Available online 14 September 2011

Keywords:
Electrodeposition
Semiconductor
Water oxidation
Conductivity
Doping

ABSTRACT

Photoelectrochemical (PEC) water oxidation using hematite (α-Fe_2O_3) is of great interest in terms of solar fuels and artificial photosynthesis. In this study, Cd-incorporated nanocrystalline hematite films (Cd–Fe_2O_3) supported on conducting glass have been prepared via co-electrodeposition of aqueous Fe(III) and Cd(II) with varying Cd:Fe atomic ratios (up to 3.2 at.%) and optimized for their PEC performances under a simulated solar light (AM 1.5-irradiation). Surface analysis indicates that the Cd co-deposition increases the hematite particle size from ca. 50 nm to 70–100 nm due to interparticle agglomeration and decreases the overall UV–Vis absorbance of hematite. X-ray photoelectron spectroscopic study also indicates that Cd incorporation shifts the binding energy of oxygen atoms to lower energy direction whereas it does not affect the binding energy of Fe 3d. This suggests that Cd exists mainly as CdO and/or $Cd(OH)_2$ in the hematite surface. When an optimal level of Cd content (~1 at.%) is electrodeposited, the photocurrent of hematite film is significantly enhanced by a factor of ca. four at $E = 1.23\ V_{RHE}$ under AM 1.5-irradiation and the photoactive spectral region is red-shifted. Electrochemical impedance spectroscopic analysis further reveals that the flat band potential of hematite is shifted by ca. −30 mV to negative potential direction and the charge transfer resistance (R_{ct}) is significantly reduced by Cd incorporation. Detailed surface analyses, optimization for preparation condition of hematite films, and discussion for PEC behaviors were described.

1. Introduction

Recently, photoelectrochemical (PEC) water oxidation has received growing attention as a mean to produce solar fuel via water splitting, which has been considered one of the grandest challenges in contemporary science [1–3]. In contrast to molecular hydrogen obtained directly or indirectly from fossil fuels, solar hydrogen produced from water has no carbon footprint [4–7], promising a sustainable hydrogen economy. PEC oxygen evolution (water oxidation), a counter reaction for hydrogen evolution (water reduction) in overall water splitting, however, suffers from lower efficiency than that of hydrogen evolution due to kinetically hindered four-electron transfer for oxygen evolution at a low power density of solar spectrum in nature [1].

Various metal oxide semiconductors including WO_3 [8,9], $BiVO_4$ [10,11], TiO_2 [12,13], and sensitized TiO_2 [14–18] have been studied for PEC water oxidation and the most suitable is iron oxide (hematite, α-Fe_2O_3) [19–27]. Hematite possesses an ideal bandgap energy of ca. 2.2 eV ($\lambda < 564$ nm) enabling absorption of ca. 40% of solar spectrum and the theoretical maximum efficiency of solar-to-hydrogen is 15% when hematite is used as a photoanode [19]. In addition, it is chemically stable in wide pH range in aqueous conditions, very abundant in nature, and cost-effective in synthesis. Despite such advantages, however, it suffers from low conductivity and fast charge recombination primarily due to extremely heavy carrier effective masses [28] and thereby short carrier diffusion length, resulting in low PEC performance. For example, TiO_2 and WO_3 have hole diffusion lengths of ~100 μm and 100–150 nm, respectively, whereas hematite has the length of only 2–4 nm [24]. This challenge has been overcome (1) by loading noble metals (e.g., Ag [29]) or depositing oxygen-evolving catalysts on hematite [30,31] and (2) by doping or incorporating various metal cations (Sn [32], Si [22,33], Ti [34–37], Al [38,39], Mo [40], Cr [38,40], Zn [36,38], Mg [38], Cu [38], Pt [41], Ta [42], V [38], Nb [43]) into hematite. The latter has attributed the dopant-induced enhancement of PEC performance primarily to increase in conductivity [37,40] and flat-band potential alternation [44]. For example, Saremi-Yarahmadi et al. [33] and Cesar et al. [22] have reported similar results that Si-doping via atomic pressure chemical vapor deposition significantly enhanced the PEC performance of hematite, while Hu et al. found that Ti and Pt are active dopants in enhancing the PEC performance [34,45]. On the other hand, Jang et al. screened effective dopants for

* Corresponding author. Tel.: +82 53 950 7371.
E-mail address: hwp@knu.ac.kr (H. Park).

0926-3373/$ – see front matter © 2011 Elsevier B.V. All rights reserved.
doi:10.1016/j.apcatb.2011.09.002

hematite with a scanning electrochemical microscopic technique and found that Ti and Sn improved the photocurrent of hematite films [38]. Although such enhancements have been ascribed to increases in conductivity and thereby inhibition of charge recombination, the detailed mechanism has not been fully understood yet.

This study reports the synthesis of cadmium(II)-incorporated hematite (Cd–Fe_2O_3 or Cd–hematite) films with varying at.% of Cd(II) (0–3.2%) and their PEC performances under a simulated solar light (AM 1.5-irradiation). Heavy doping of Cd into Fe_2O_3 lattice with 1:2 atomic ratio of Cd:Fe have been known to create magnetic spinel ferrites of $CdFe_2O_3$, which are widely used in gas sensors, electronic devices, and information storage [46–48]. Such Cd doping (or alloying) significantly increases the electrical conductivity of Fe_2O_3 by a minimum of three orders of magnitude (e.g., 10^{-14} to $10^{-7}\,\Omega^{-1}\,cm^{-1}$ with Fe_2O_3 to $\sim 10^{-4}\,\Omega^{-1}\,cm^{-1}$ with $CdFe_2O_3$) [47,48] as well as changes the surface properties of Fe_2O_3 [49]. In this study, hematite has been prepared as via an electrodeposition reported elsewhere [26,50], which has been known to be very facile for in situ preparing reproducible and robust hematite and metal-incorporated hematite films on conducting glass substrate. It has been found that electrodeposition of Cd significantly enhances the water oxidation current (I_{ph} at 1.23 V vs. RHE) by a factor of maximum four under an optimal condition. Despite significantly low and non-stoichiometric content of Cd (up to 3.2 at.%), the electrical conductivity of hematite films significantly increases and even their PEC performances are boosted up by Cd incorporation. To the best of our knowledge, such enhancement of PEC performance of hematite by Cd has been not reported yet.

2. Experimental details

2.1. Preparation of pure and Cd-incorporated hematite films

A typical electrodeposition method was employed to deposit hematite films onto fluorine-doped tin oxide (SnO_2:F) conducting glass (FTO; Pilkington TEC) substrates. FTO was cut into small pieces of 1.5 cm × 3.0 cm which were cleaned with distilled water and ethanol sequentially. Then, they were immersed in an aqueous solution containing $FeCl_3{\cdot}6H_2O$ (5 mM, Aldrich), NaF (5 mM, Aldrich), NaCl (0.1 M, Aldrich) and H_2O_2 (1 M, Aldrich), to which various potential cycles were applied from −0.52 to +0.41 V vs. SCE (saturated calomel electrode) [26] at a scan rate of 0.1 V/s (Versastat 3-400) with a platinum gauze as a counter electrode. After electrodeposition, the films were rinsed with distilled water to remove precursor residues at the surface and were annealed in the presence of air at various temperatures from 400 to 700 °C for 30 min. The electrodeposited hematite films are yellowish and quite transparent, and post-annealing changes their color to dark-red (Fig. S1 in Supporting Material). For Cd-incorporated hematite films, FTO glass was immersed in the hematite precursor solution with cadmium acetate of varying Cd atomic ratios (0, 2, 5, 8, 10, and 15%) with respect to Cd + Fe. An energy-dispersive X-ray spectroscopy (EDX) analysis indicated that the actual amounts of deposited Cd were approximately 0, 0.40, 0.75, 0.95, 1.45, and 3.20%, respectively (Fig. S2 in Supporting Material). The other conditions for electrodeposition and heat treatment were identical to those of hematite films. In addition, Cd electrodeposition was performed with the hematite-coated FTO substrates to investigate the co-electrodeposition effect of Cd on the PEC performance of hematite (i.e., co-deposition vs. sequential deposition).

2.2. Surface characterizations

In order to check the crystalline structures of as-prepared samples, X-ray diffraction (XRD) analyses were carried out with an X-ray diffractometer (Rigaku D, Max-2500) employing Cu Kα radiation (λ = 0.15406 nm) with 40 kV and 100 mA at a 0.02° scan rate. Scanning electron microscopy (SEM) was performed using an S-4800 (Hitachi) with energy dispersive spectrometry (EDS) to obtain the surface at.% of Cd in Cd–Fe_2O_3 films. The surface atomic composition and states of the samples were determined by X-ray photoelectron spectroscopy (XPS, Kratos, XSAM 800 pci) using the Mg Kα line (λ = 1253.6 eV) as the excitation source. The binding energies of Fe2p, Cd3d, and O1s were referenced against the C1s. The optical property of the films was characterized by a UV–Vis spectrophotometer (T60U, PG Instruments) and a UV–Vis diffuse reflectance spectrophotometer (Shimadzu UV2450).

2.3. Photoelectrochemical tests

The photoelectrochemical (PEC) measurements of hematite and Cd–Fe_2O_3 films were conducted in a standard three-electrode cell (single cell) using an SCE reference electrode and a platinum gauze counter electrode with an aqueous electrolyte solution of 1 M NaOH (pH ∼13.5). Light was irradiated from a solar simulator equipped with an air mass filter 1.5 (LS-150 Xe, ABET) to the back side of the hematite and Cd–Fe_2O_3 films (i.e., FTO side) with a photo-active area of 0.95 cm^2 in contact with the electrolyte. When necessary, various long-wave band pass filters were placed between the light source and the sample electrode. Onset potentials were determined by comparing cyclic voltammograms of electrodes in the dark and under irradiation, while open circuit potentials were obtained by using software in effect functioned as a zero-resistance ammeter. For Nyquist plots, AC impedance measurements of the films were carried out in a 1 M NaOH solution with a frequency range of 100 Hz to 0.01 Hz with an AC voltage of 10 mV RMS (Gamry Instruments REF600-03068) in the dark and under AM-1.5 light. In order to estimate flat band potentials of hematite and Cd–hematite, the Mott–Schottky analyses were also carried out by CompactStat (Ivium) at 1 kHz to 1 Hz in a 1 M NaOH solution by scanning the potential range from +0.5 V to −1.5 V with a scan rate of 10 mV s^{-1}.

3. Results and discussion

3.1. Surface characterization of hematite and Cd–Fe_2O_3 films

Fig. 1a shows the effect of Cd deposition on the XRD patterns of iron oxide film deposited on conducting glass (SnO_2:F-coated glass) substrates. From the XRD peak analysis, it is obvious that iron oxide calcined at 650 °C has hematite (α-Fe_2O_3) crystal structure (2θ = 24.14° (012), 33.15° (014), 35.61° (110), 39.28° (006), 40.86° (113), 43.52° (202), 49.48° (024), 54.09° (116), 56.15° (211), 57.59° (018), 62.45° (214), 63.99° (300), and 66.10° (128); the numbers in parentheses refer to Miller indices) and the hematite structure is maintained in Cd–Fe_2O_3. Other crystal structures of Cd and Cd–Fe hybrid oxides (e.g., $CdFe_2O_4$), even if present, were not found in the XRD patterns, which is likely due to low Cd content with respect to Fe. Fig. 1b presents UV–Vis absorption spectra of hematite and Cd–Fe_2O_3 films (FTO base). It is obvious that irrespective of Cd at.%, two broad but distinct absorption bands centered at ca. 410 nm and 530 nm are found. Such bands are attributed to LMCT ($^6A_1 \rightarrow {}^4T_2$ or ^4E; transition from O2p to Fe3d) and ligand field transition ($2(^6A_1) \rightarrow 2(^4T_1)$), respectively [19]. Among these two transitions, the LMCT is primarily responsible for the visible light absorption of hematite. Also, Fig. 1b shows that the overall absorbance of λ < ca. 600 nm decreases with increasing Cd at.%, whereas no apparent correlation between the absorbance and the Cd at.% in the range of λ > ca. 600 nm was obtained. This is likely due to several factors such as the scattering effect of hematite particles with different particle sizes depending on Cd at.%. The decreases in

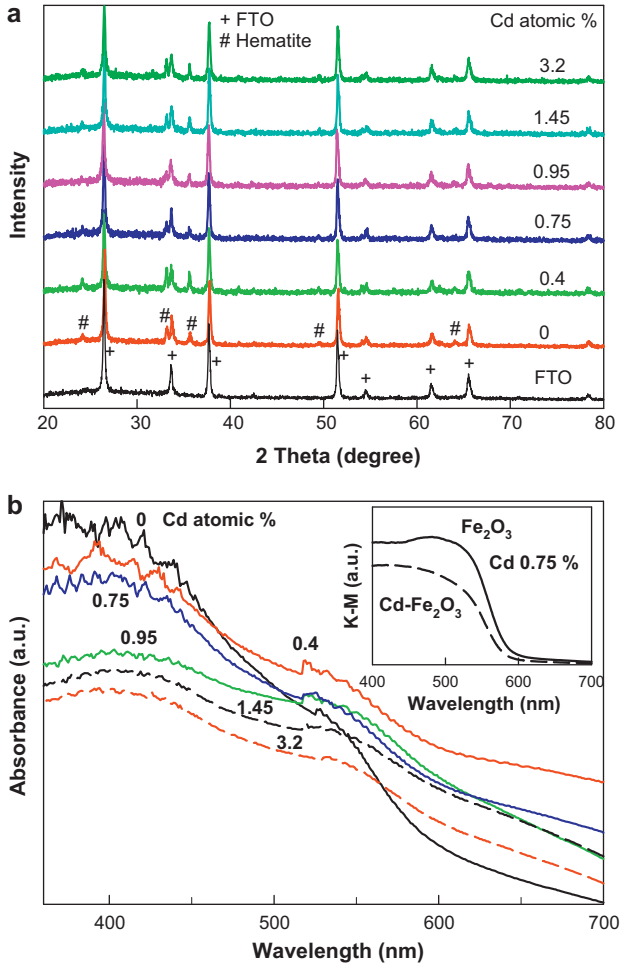

Fig. 1. (a) XRD patterns of Fe_2O_3 and Cd–Fe_2O_3 films with different Cd at.% (=Cd/(Cd + Fe) × 100). All the films were annealed at 650 °C for 0.5 h in the presence of air. (b) UV–Vis absorption spectra of Cd–Fe_2O_3 films deposited on fluorine-doped SnO_2 (SnO_2:F) substrate with varying Cd at.%. Inset shows UV–Vis diffuse reflectance absorption spectra (expressed as a Kubelka–Munk unit) of hematite and Cd–Fe_2O_3 films with Cd of 0.75 at.%.

absorbance of λ < ca. 600 nm were proven further by a comparison of diffuse reflectance absorption spectra between hematite and Cd (0.75%)–Fe_2O_3 films (Fig. 1b, inset). Similar to Cd, Cr and Mo also decrease the absorbance of hematite film [40] whereas Al increases the absorbance as compared to bare hematite films [39]. This indicates that the optical properties of hematite and modified hematite films are very sensitive to surface status and quite difficult to fully understand and rationalize. Fig. 2 displays scanning electron microscopic (SEM) images of hematite and Cd–Fe_2O_3 films annealed at 650 °C for 0.5 h. Bare hematite is composed of fine and uniform particles with ca. 50 nm in diameter while Cd-deposition increases the particle size to ca. 70–100 nm via a particle-to-particle interconnection and merging process (Fig. 2a–d). Such an agglomeration effect of hematite particles has been typically observed when hematite films were prepared via electrodeposition in the presence of Al [39], Pt [45], Mo [40], and Cr [40] cations. This indicates that the metal cations including Cd play a role as a nucleic or catalytic site for interparticle aggregation. Fig. 2e and f also compare the side views of bare hematite and Cd–Fe_2O_3 films. It is obvious that hematite particles deposited on an FTO layer of ca. 500 nm form a layer of 1.5–1.8 μm thickness along with a highly porous structure and the Cd–Fe_2O_3 film has a similar porous configuration with a layer thickness of 1.3–1.8 μm. This porous structure is very beneficial for high photon-to-current efficiency due to photon-confinement and multiple scattering of incident photons inside of hematite film.

XPS analyses of hematite and Cd–Fe_2O_3 films were performed in order to investigate the electronic states of component elements. As displayed in Fig. 3a, two characteristic bands for Fe^{3+} were shown at ca. 711 eV ($Fe2p_{3/2}$) and ca. 724 eV ($Fe2p_{1/2}$). An Fe^{2+} shakeup satellite band (ca. 715 eV) was not found, indicating that the as-prepared iron oxide films have Fe^{3+} as a primary iron species. $Cd3d_{5/2}$ bands were also shown at ca. 405 eV (Fig. 3b) which corresponds to CdO or $Cd(OH)_2$. Yet, those bands of Cd–Fe_2O_3 samples with Cd < 0.75% were scarcely observed which is likely due to a thinness of the films and/or lower Cd content than expected. For a more detailed study on the chemical states of Fe and Cd, XPS spectra of O1s for hematite and Cd–Fe_2O_3 films were compared (Fig. 3c–f). Overall, the spectra of O1s are quite similar (Fig. 3c) but their binding energies were shifted to a lower energy direction by 0.2–0.4 eV by Cd incorporation. Since typical binding energies of oxygen atoms coordinated to Cd(II) are slightly lower than those coordinated to Fe(III), the O1s spectra were deconvoluted with respect to oxygen atoms coordinated to Fe(III) for bare hematite and oxygen atoms coordinated to Fe(III) and Cd(II) for Cd–Fe_2O_3. As shown in Fig. 3d–f, hematite has three different oxygen atoms: Fe_2O_3 (529.6 eV), Fe(OH)O (531.2 eV), and FeOOH (531.9 eV) (Fig. 3d). Meanwhile Cd–Fe_2O_3 has two additional oxygen atoms coordinated to Cd: CdO (529.5 eV) and $Cd(OH)_2$ (532.8 eV) (Fig. 3e and f). The iron oxide hydroxides (Fe(OH)O and FeOOH) in bare and Cd–Fe_2O_3 samples are likely goethite (α-FeOOH) since it is the most thermodynamically stable iron oxide at ambient temperatures [19]. The intensity ratio of Fe(OH)O and FeOOH was estimated to be lower than 1 with Cd (0.75%)–hematite (Fig. 3e) whereas it became greater than 1 with Cd (1.45%)–hematite (Fig. 3f). This indicates that the introduction of Cd somehow affected the electronic states of the iron oxide hydroxides. It should be pointed that the relative intensity of Fe_2O_3 with respect to the iron oxide hydroxides decreased with increasing Cd content. This seems to be quite acceptable since a large amount of Cd incorporation may break the hematite structure and even change it into other structures. Similar to Fe, the incorporated Cd(II) species is also readily transformed into oxide/hydroxides in an aqueous phase when other strong paring elements, such as S or Se, are not present [51,52]. The Cd(II) can exist as two states: doped vs. surface one. The former is obtained when Cd atom replaces Fe atom in the hematite lattice (cation–cation substitution) while the latter is achieved when Cd is present on the hematite surface. In either case, the incorporated Cd(II) should exist as a CdO and/or $Cd(OH)_2$ (i.e., >Fe–O–Cd–OH; >Fe denotes surface Fe). The larger size of the Cd ion (1.69 Å) than the Fe ion (1.34 Å) in their covalent radii [53] suggests that the substituted Cd may reduce a photo-stability of hematite under prolonged irradiation condition.

3.2. *Photoelectrochemical performances of hematite and Cd–Fe_2O_3 electrodes*

Prior to the investigation of PEC performances of Cd–Fe_2O_3 electrodes, the electrodeposition conditions of hematite films were varied in order to optimize them and obtain reliable and higher effects. Firstly, the cycle numbers of cyclic voltammogram (CV) (−0.52 V_{SCE} to +0.41 V_{SCE}) for growing hematite films were changed in the range of 50–200 and then annealed identically at 550 °C for 30 min in the presence of air. This preliminary experiment indicated that a CV cycle number of above 100 has no significant effect on the *I–V* patterns and photocurrent generations of hematite electrodes (Fig. S3 in Supporting Material). Since the CV cycle number determines the thickness of hematite films, a film thicker than a certain level of thickness should have a reduced photon penetration and a decrease of interfacial charge transfer reaction with electrolyte.

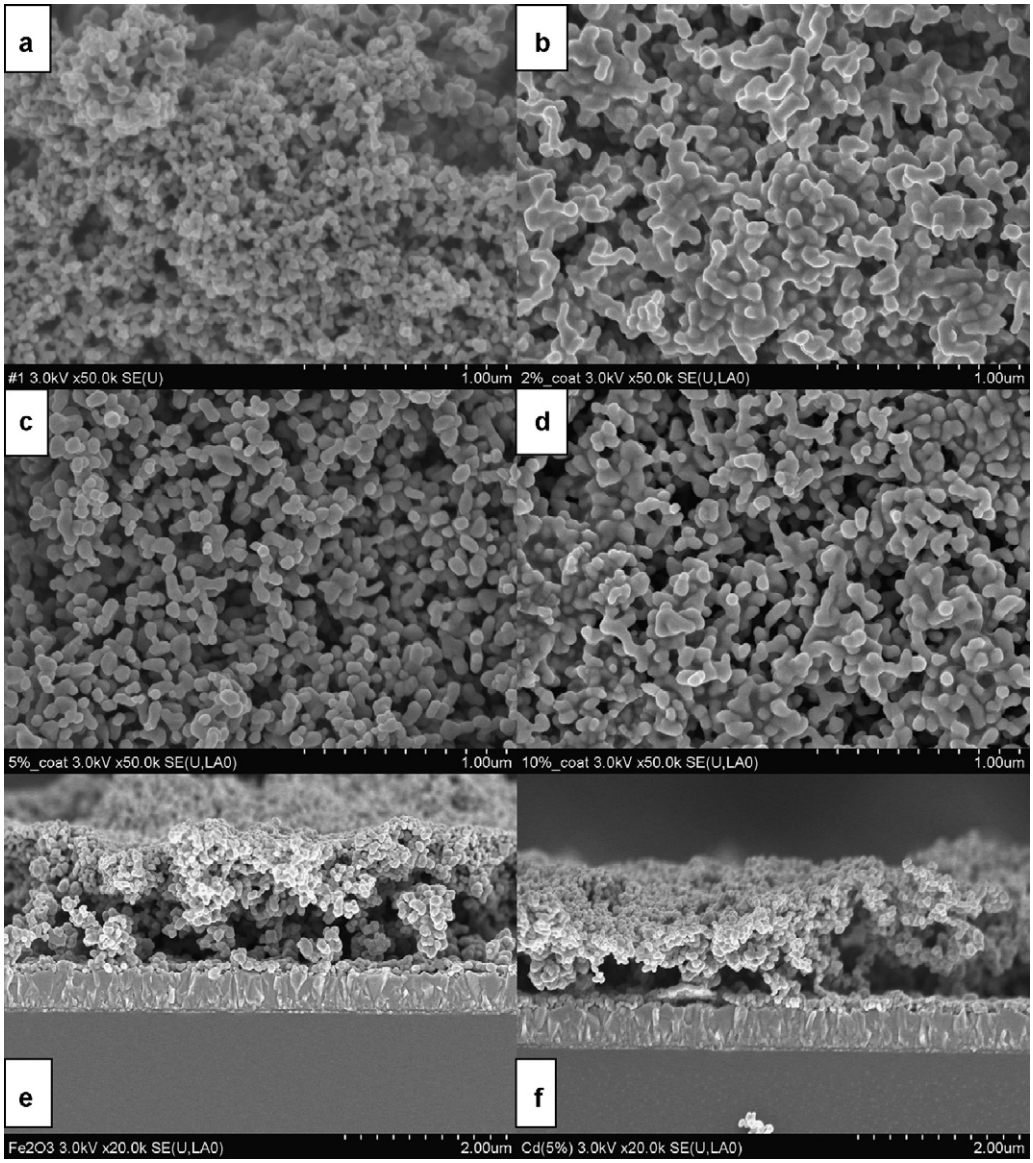

Fig. 2. SEM images (top views) of Cd–Fe_2O_3 films with different Cd at.%. (a) 0% (i.e., hematite), (b) 0.4%, (c) 0.75% and (d) 1.45%. SEM images (side views) of (e) bare hematite and (f) Cd (0.75%)–Fe_2O_3 films. In e and f, top layer: hematite, middle layer: FTO (SnO_2:F) and bottom layer: glass substrate.

In this study, hematite films (100-cycle) have been found to have a thickness of ca. 1.7 μm (Fig. 2e and f). Secondly, annealing temperatures also were changed from 400 to 700 °C. As shown in Fig. 4a, despite the same electrodeposition condition with 100-cycle, the post-annealing temperature significantly affects *I–V* patterns of irradiated hematite electrodes. For example, a hematite electrode annealed at 400 °C (hematite@400) has a very low current even at a high overpotential of ca. 1 V_{SCE} as compared to the theoretical water oxidation potential ($E^0(O_2/H_2O)$ = 1.23 V_{RHE} = 0.193 V_{SCE} at pH 13.5) (reaction 1).

$$2H_2O \rightarrow O_2 + 4H^+ + 4e^- \quad (E = 1.23\,V_{RHE}) \tag{1}$$

However, the photocurrent becomes greater with increasing annealing temperature, reaches the greatest at hematite@650, and then decreases at hematite@700. It is of note that hematite electrodes annealed at over 400 °C have two separate potential regions: photoelectrochemical (E < ca. 0.7 V_{SCE} = 1.737 V_{RHE}) vs. catalytic regions (E > ca. 0.7 V_{SCE}). The former corresponds to the four-electron water oxidation (reaction (1)) whereas the latter is likely associated with two-electron water oxidation (reaction (2)), as well as the thermodynamic water oxidation in the dark (reaction (1)).

$$2H_2O \rightarrow H_2O_2 + 2H^+ + 2e^- \quad (E = 1.776\,V_{RHE}) \tag{2}$$

Hence, the hematite electrodes obtained at 650 °C (hematite@650) should have better catalytic and superior PEC performances than hematite@400. Fig. 4b also compares the differences between dark potentials and photopotentials as a function of annealing temperature. The gradual increase of potential difference is ascribed to the improved crystallinity of hematite films at higher temperatures and the sudden decrease at 700 °C is likely due to the crystallinity change of fluorine-doped tin oxide (FTO) substrate and consequently decrease in its conductivity [39,40]. Therefore, other conducting substrates, such as Pt and Ti, are often used for annealing hematite films above 650 °C [41,54]. On the basis of the above results, all the following Cd–Fe_2O_3 films were prepared with a fixed experimental condition (100-cycles; 650 °C for 30 min).

Fig. 5 shows the effects of Cd at.% on the *I–V* patterns that were obtained from cyclic voltammograms (3 cycles), and photocurrent generations of Cd–Fe_2O_3 electrodes. It is apparent that Cd

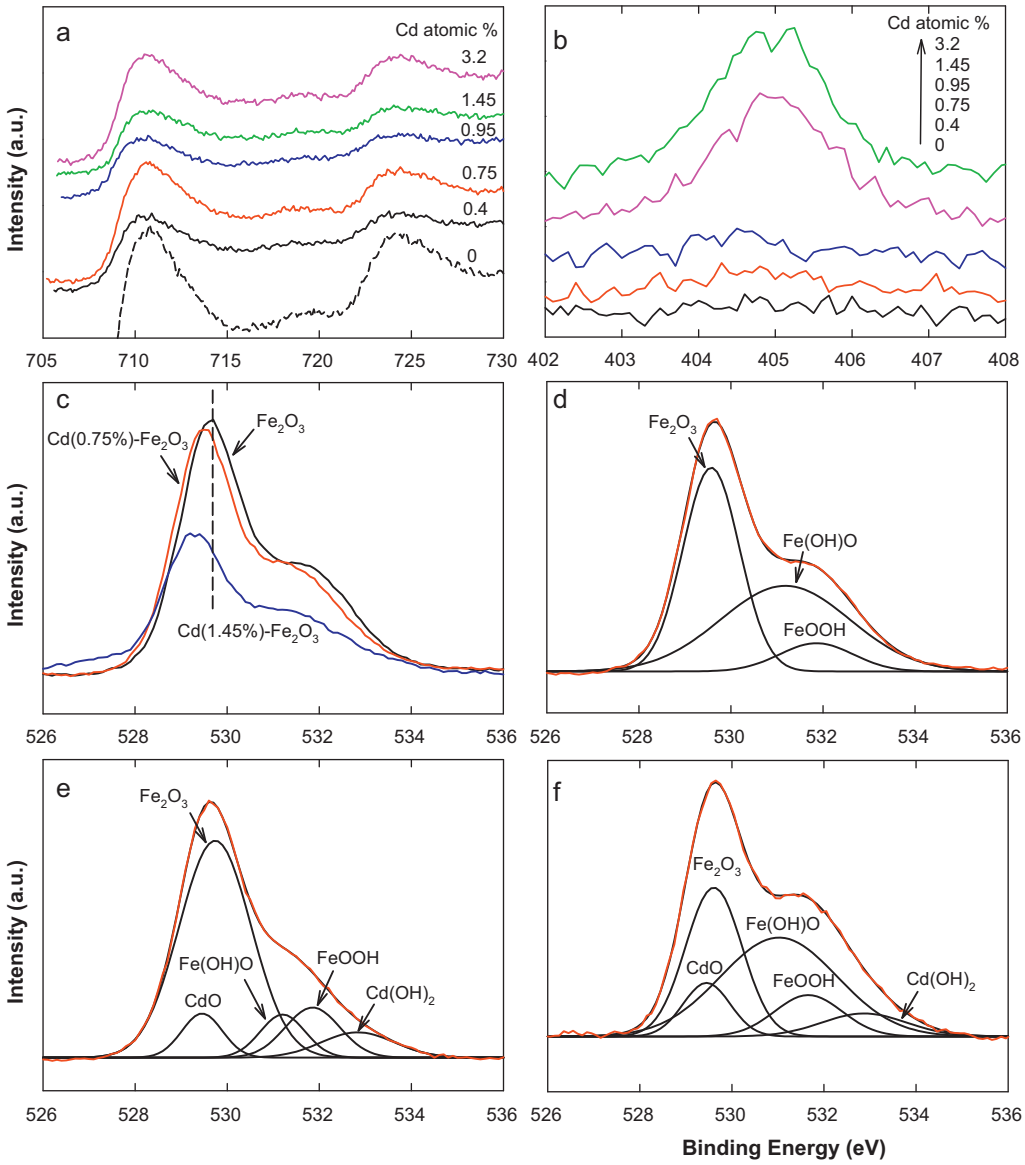

Fig. 3. XPS spectra of (a) Fe2p and (b) Cd3d for Cd–Fe_2O_3 films with different Cd at.%. (c) XPS spectra of O1s for bare hematite and Cd–Fe_2O_3 films with Cd at.% of 0.75 and 1.45. Deconvoluted XPS spectra of O1s for (d) bare hematite, (e) Cd (0.75%)–Fe_2O_3, and (f) Cd (1.45%)–Fe_2O_3 films.

deposition enhances the photocurrent generation as compared to bare hematite. Such enhancement is highest with a Cd content of around 1 at.% and a heavy Cd content of ~3 at.% decreases the photocurrent. Open circuit potentials (OCPs) of the electrodes also indicate that hematite electrodes with a Cd content of less than 1.5 at.% have more negative OCPs of −0.36 to −0.45 V_{SCE} than bare hematite with OCP of −0.32 V_{SCE} (Fig. S4 in Supporting Material). Yet, the OCP of Cd (3.2%)–Fe_2O_3 decreases to ca. −0.23 V_{SCE}. However, irrespective of Cd content, the photocurrent onset potentials (ca. −0.13 V_{SCE}) estimated from the CV patterns are not much different from those of bare hematite (see Table 1). Also, as shown in Fig. 5b, the hematite electrodes generate a maximum four-fold greater photocurrent at $E = 0.193\ V_{SCE}$ (1.23 V_{RHE}) when Cd of around 1 at.% is co-electrodeposited. The application of overpotential as large as 0.8 V_{SCE} (1.837 V_{RHE}) generates greater currents and these higher currents, as indicated above, might be due to the combined effect of oxygen evolution and formation of hydrogen peroxide (Fig. 5c and reactions (1) and (2); see also Fig. S5 in Supporting Material). It has been found that such enhanced photocurrent by Cd incorporation was maintained over 12 h at a bias potential of 1.23 V_{RHE} under intensified AM 1.5-light (4 Sun, 400 mW/cm^2) and repetitive use of Cd–hematite electrodes did not cause PEC deactivation. Finally, we have checked PEC performances of bare hematite and Cd–Fe_2O_3 electrodes as a function of cut-off wavelengths by inserting different long-wave pass filters between the light source and the PEC cell. As shown in Fig. 6, the photocurrents of bare hematite electrodes decrease with longer-wave pass filters, which are still measurable at a 550 nm-pass filter and are virtually zero at a 610 nm-pass filter. This indicates that the bandgap of hematite in terms of photocurrent generation (i.e., photogeneration of conduction band electron) is estimated to be ca. 2.25 eV (E_g (eV) = $h\nu/\lambda$ = 1240/550). In the case of Cd–Fe_2O_3 the photocurrents

Table 1
Effect of Cd (0.75%) deposition on flat band potentials (V_{SCE}) of hematite film.

Sample	Mott–Schottky plot	Photocurrent onset potential	Open circuit potential
Pure hematite	−0.80	−0.094	−0.32
Cd–hematite	−0.85	−0.129	−0.39

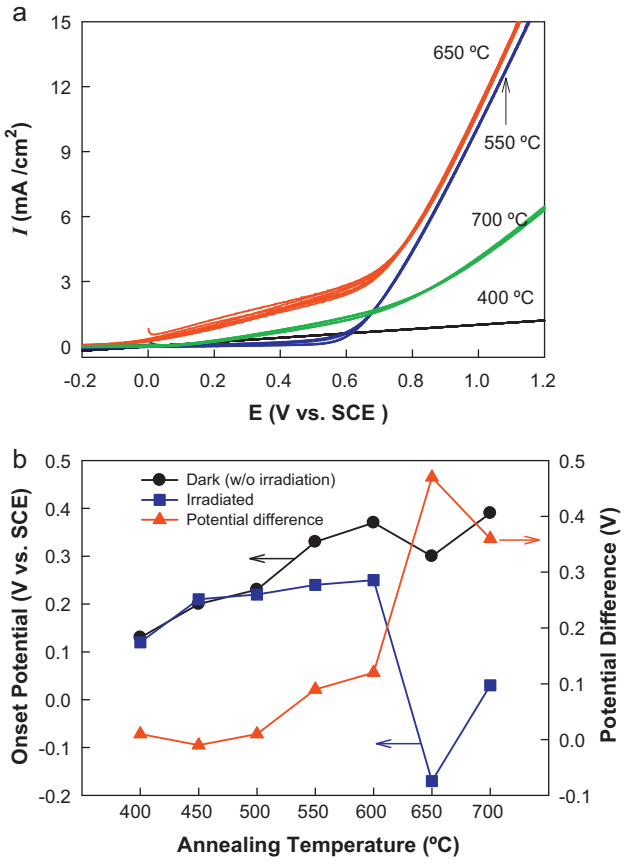

Fig. 4. Effects of annealing temperatures on (a) *I–V* curves of hematite films under AM 1.5-irradiation (scan rate, 0.1 V/s) and (b) the (dark) potentials, photopotentials (under AM 1.5-irradiation), and their differences.

are enhanced 3–4 fold irrespective of cut-off wavelengths and such enhancement is still maintained with >550 nm-pass filters. Note that a certain level of photocurrent is generated even with 610 and 665 nm-pass filters, which might arise from the photoexcitation of hematite, as well as surface CdO with a varying bandgap of 1.0–2.35 eV [55].

3.3. Roles of Cd in PEC performances of hematite films

As described in the aforementioned sections, the incorporated Cd(II) was speculated to exist as CdO and/or $Cd(OH)_2$. Similarly to our speculation, Pt(IV)-incorporated hematite films that were prepared via co-electrodeposition also had PtO_2 on their surfaces [45]. In order to investigate the role of the CdO and $Cd(OH)_2$ in a more detailed way, we compared PEC performances of co-electrodeposited hematite and sequentially electrodeposited hematite films with Cd(II). As shown in Fig. 7, the sequential electrodeposition with annealing at each step (i.e., line 2: hematite electrodeposition → annealing → Cd electrodeposition → annealing) resulted in a slightly lower PEC performance than the co-electrodeposition (line 4) and yet a significantly higher performance than the simple hematite electrodeposition (line 1) (Fig. 7b). Since the condition of line 2 could create CdO and $Cd(OH)_2$ only on the pre-crystallized hematite surface, the enhanced PEC performance of Cd co-electrodeposited hematite should result mostly from surface CdO and $Cd(OH)_2$ as a form of ≻Fe–O–Cd–OH. No PEC performance of Cd/hematite electrodes (line 3: hematite electrodeposition → Cd electrodeposition → annealing) is due to peeling away of the unannealed hematite particles from the FTO substrate during the Cd electrodeposition.

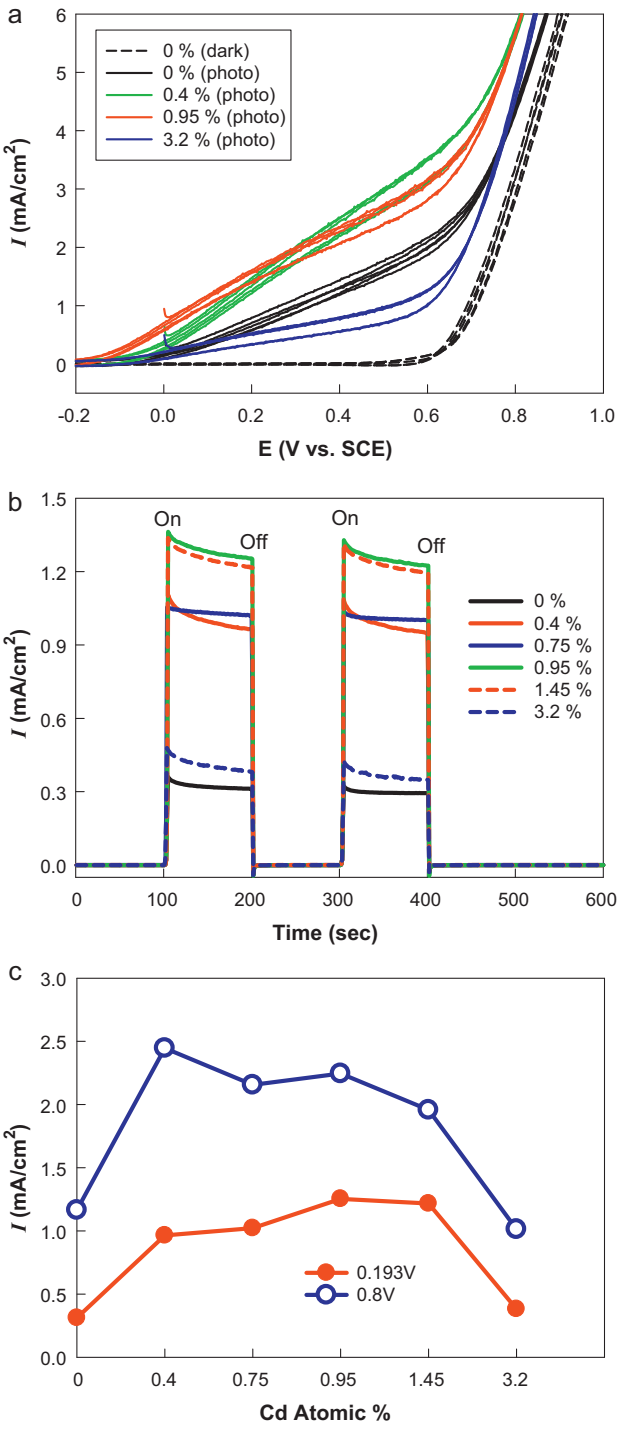

Fig. 5. (a) *I–V* curves of Cd–Fe_2O_3 films with different Cd at.% in the dark and under AM 1.5-irradiation. (b) Photocurrent generations of Cd–Fe_2O_3 films as a function of Cd at.% at $E = 0.193\ V_{SCE}$ (i.e., $1.23\ V_{RHE}$). (c) Effects of Cd at.% on the photocurrent generations at $E = 0.193$ and $0.8\ V_{SCE}$. Electrolyte: 1 N NaOH.

The roles of the incorporated Cd(II) might be multiple. First, the Cd(II) can assist the electrocatalytic oxygen evolution reaction occurring at hematite surface (reaction (3)) [56,57]. This role is similar to those of metal oxide catalysts, such as IrO_2, PtO_2, and RuO_2 [56,58], which reduce activation energy for oxygen evolution and facilitate electron transfer kinetically.

$$\succ Cd\text{–}OH + OH^- \rightarrow \succ CdO + H_2O + e^- \quad \text{(in alkaline condition)} \tag{3}$$

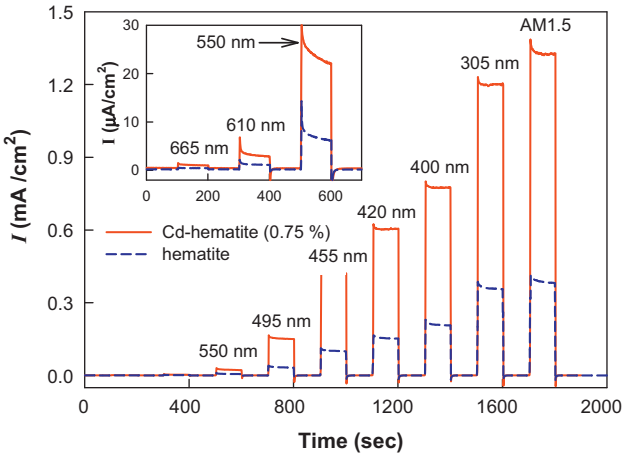

Fig. 6. Effects of long-wave pass filters on the photocurrent generations of bare hematite and Cd (0.75%)–Fe_2O_3 films. Inset shows the magnified photocurrent generations in the cases of 550, 610, and 665 nm-pass filters. Electrolyte: 1 N NaOH.

Second, the incorporated Cd(II) can assist the photoelectrochemical water oxidation reaction. CdO is known for being a semiconducting oxide with a bandgap energy of ca. 1.0–2.35 eV [55]. Hence it can contribute to the generation of electron–hole pairs although the degree of contribution is difficult to quantify. The third role is

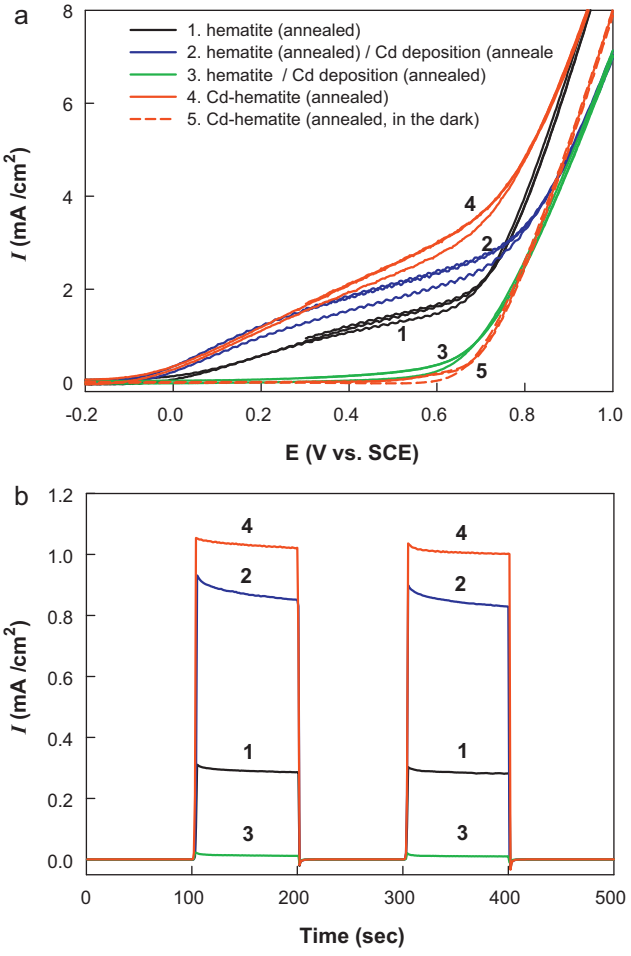

Fig. 7. Comparison of Cd-codeposited hematite and Cd-postdeposited hematite electrodes for (a) their *I–V* behaviors and (b) photocurrent generations at $E = 0.193\ V_{SCE}$. All the annealing conditions are identically 650 °C for 0.5 h. For line numbers in b, see legend in a. Electrolyte: 1 N NaOH.

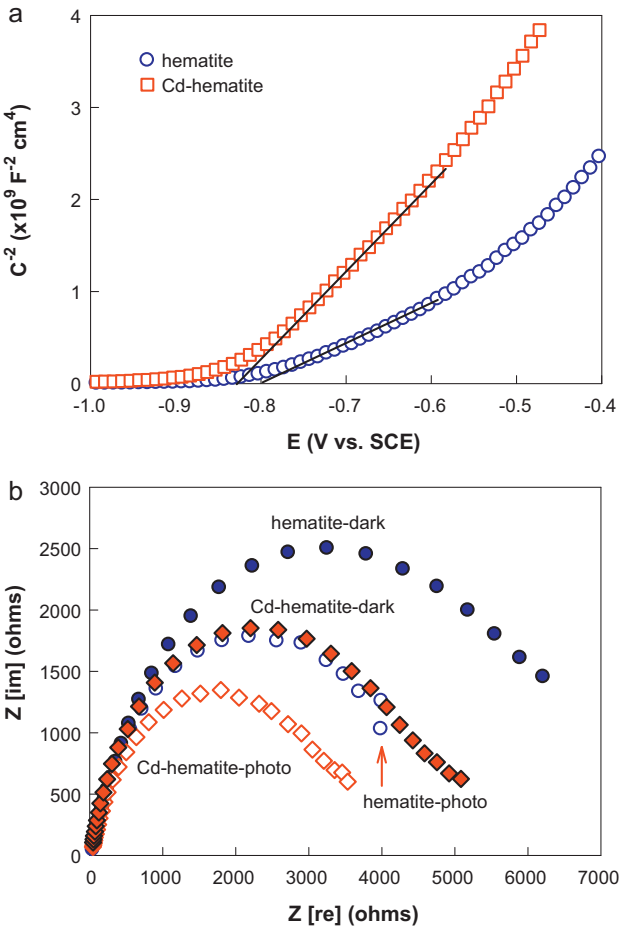

Fig. 8. (a) Mott–Schottky plots of hematite and Cd (0.75%)–hematite electrodes at the frequency of 1 kHz in 1 N NaOH. (b) Nyquist plots for bare hematite and Cd (0.75%)–Fe_2O_3 films in 1 N NaOH solution in the dark and under AM 1.5-irradiation.

to passivate the surface state of hematite particles. The hematite surface usually has many trapping states where charge recombination mostly occurs due to short charge carrier diffusion lengths. Thus reducing the trapping states or blocking the surface states with oxide layers (e.g., Al_2O_3 and SnO_2) can enhance the PEC performance of hematite [59,60]. The CdO can generate a similar effect.

The incorporated Cd(II) can also affect the energetics of hematite by changing Fermi level and flat band potential. Hence, we have performed Mott–Schottky analyses of hematite and Cd–hematite electrodes (Fig. 8a). It seems that both electrodes fall into the depletion region at $E <$ ca. $-0.8\ V_{SCE}$ and thus the slopes of linear region ranging between $-0.6\ V_{SCE}$ and $-0.8\ V_{SCE}$ were used to estimate the flat band potentials of the electrodes. Apparently Cd electrodeposition shifts the flat band potential of hematite from $-0.8\ V_{SCE}$ to $-0.83\ V_{SCE}$. Such a shift into a negative potential region was also verified by the analyses of photocurrent onset potentials and open circuit photopotentials (Table 1). The more positive values in the photocurrent onset potentials and open circuit photopotentials as compared to the flat band potentials obtained from the Mott–Schottky plots resulted from surface recombination [61].

The Cd(II) also can modulate the bandgaps of oxide semiconductors and shift their absorption band to the mostly visible light region. In the case of hematite, however, such effect was less obvious due to its intrinsic capability of absorbing visible light and easy perturbation of the bandgap by film thickness [27] and surface treatment [23]. In this study, the absorbance of Cd–Fe_2O_3 was lower than or similar to that of bare hematite in the range of $\lambda < 520$ nm (Fig. 1b) with a similar film thickness (Fig. 2e and f).

Nevertheless, the irradiation of $\lambda > 550$ nm (the photo-inactive region of hematite; see Fig. 6) generates an additional photocurrent of ca. 20 μA/cm^2 at Cd–Fe_2O_3 film. This suggests that the change of optical property by Cd incorporation may contribute to enhancing the photocurrent generation of hematite electrode in a moderate level.

An alternative effect of Cd incorporation is likely to increase the conductivity of hematite thus increasing the charge carrier mobility and reducing the charge recombination. In fact, most metal dopants that enhance the PEC performance of hematite have been speculated to increase the conductivity of hematite [29,33,34,37–40,44,45,62,63]. In order to check the electrical conductivities of hematite and Cd–Fe_2O_3, the electrochemical impedance spectroscopy (EIS) analyses of both films were carried out. The photoelectrochemical cell was considered to represent an equivalent circuit of two resistors (solution and electrode) and a single capacitor (electrode). As displayed in the Nyquist plots of Fig. 8b, hematite and Cd–Fe_2O_3 have similar semicircles with different radii. The fittings for the semicircles indicate that hematite has charge transfer resistances (R_{ct}) of 6690 Ω with differential capacitance of double layer (C_{dl}) of 5.06×10^{-5} F in the dark and 4460 Ω (C_{dl}: 7.84×10^{-5} F) under AM 1.5-irradiation. Such a decrease in R_{ct} (i.e., photo-induced increase in conductivity) is a typical property of semiconducting materials. Meanwhile R_{ct} of Cd–Fe_2O_3 in the dark is significantly reduced to 5130 Ω (C_{dl}: 2.16×10^{-5} F) as compared to bare hematite and is further reduced to 3730 Ω (C_{dl}: 4.39×10^{-5} F) upon light irradiation. The mechanism for the conductivity of hematite and its enhancement by Cd incorporation can be summarized with the following:

$$Fe^{3+} + e^- \rightarrow Fe^{2+} \quad (4)$$

$$O \rightarrow 0.5O_2 + V_O{}^{2+} + 2e^- \quad (5)$$

$$Cd^{2+} + e^- \rightarrow Cd^{+} \quad (6)$$

where $V_O{}^{2+}$ is oxygen vacancies. The conductivity of hematite arises from electron transport as in reactions (4) and (5) while the incorporated Cd might accept additional electrons improving the conductivity of hematite (reaction (6)). Light irradiation generates more electron–hole pairs and increases the mobility of charge carriers.

4. Conclusions

This study showed that the co-electrodeposition of Fe(III) and Cd(II) results in Cd-incorporated nanocrystalline hematite films with a high porosity and uniform particle size. It has been demonstrated that Cd incorporation with 0.4–1.45 at.% enhances the photoelectrochemical performances of hematite such that the photocurrent at $E = 1.23\ V_{RHE}$ is increased by a factor of max. 4 and the photoactive wavelength window is extended to 665 nm. Such enhancement likely results from the mixed effects of a shift of the flat band potential, a change in bandgap energy and an increase in conductivity. Surface characterization and thorough PEC study suggest that the incorporated Cd most likely exists as CdO (and/or $Cd(OH)_2$), which increase the conductivity of hematite and play electrocatalytic and photoelectrocatalytic roles. The employed co-electrodeposition technique is very easy to operate and reliable to get reproducible thickness of nanocrystalline hematite films, promising synthesis of metal-incorporated hematite films on various supporting substrates.

Acknowledgments

This research was supported by Basic Science Research Program (No. 2009-0071350, 2009-0089904, 2010-0002674) and by the Korea Center for Artificial Photosynthesis (NRF-2009-C1AAA001-2009-0093879) through the National Research Foundation of Korea (NRF) funded by the Ministry of Education, Science and Technology.

Appendix A. Supplementary data

Supplementary data associated with this article can be found, in the online version, at doi:10.1016/j.apcatb.2011.09.002.

References

[1] M.G. Walter, E.L. Warren, J.R. Mckone, S.W. Boettcher, Q. Mi, E.A. Santori, N.S. Lewis, Chem. Rev. 110 (2010) 6446–6473.
[2] T.R. Cook, D.K. Dogutan, S.Y. Reece, Y. Surendranath, T.S. Teets, D.G. Nocera, Chem. Rev. 110 (2010) 6474–6502.
[3] A.J. Bard, M.A. Fox, Acc. Chem. Res. 28 (1995) 141–145.
[4] X.Y. Chen, S. Shen, L. Guo, S.S. Mao, Chem. Rev. 110 (2010) 6503–6570.
[5] H. Park, C.D. Vecitis, W. Choi, O. Weres, M.R. Hoffmann, J. Phys. Chem. C 112 (2008) 885–889.
[6] H. Park, C.D. Vecitis, M.R. Hoffmann, J. Phys. Chem. A 112 (2008) 7616–7626.
[7] H. Park, C.D. Vecitis, M.R. Hoffmann, J. Phys. Chem. C 113 (2009) 7935–7945.
[8] H. Wang, T. Lindgren, J. He, A. Hagfeldt, S.E. Lindquist, J. Phys. Chem. B 104 (2000) 5486–5696.
[9] H. Wang, T. Deutsch, J.A. Turner, J. Electrochem. Soc. 155 (2008) F91–F96.
[10] A. Kudo, K. Omori, H. Kato, J. Am. Chem. Soc. 121 (1999) 11459–11467.
[11] K. Sayama, A. Nomura, Z. Zou, R. Abe, Y. Abe, H. Arakawa, Chem. Commun. 290 (2003) 8–2909.
[12] Y. Liu, B. Zhou, J. Li, X. Gan, J. Bai, W. Cai, Appl. Catal. B 92 (2009) 326–332.
[13] H. Park, A. Bak, Y.Y. Ahn, J. Choi, M.R. Hoffmann, J. Hazard. Mater. (2011), doi:10.1016/j.jhazmat.2011.1005.1009.
[14] W.J. Younpblood, S.H.A. Lee, Y. Kobayashi, E.A. Hernandez-Pagan, P.G. Hoertz, T.A. Moore, A.L. Moore, D. Gust, T.E. Mallouk, J. Am. Chem. Soc. 131 (2009) 926–927.
[15] G.B. Saupe, T.E. Mallouk, W. Kim, R.H. Schmehl, J. Phys. Chem. B 101 (1997) 2508–2513.
[16] H. Park, E. Bae, J.-J. Lee, J. Park, W. Choi, J. Phys. Chem. B 110 (2006) 8740–8749.
[17] H. Park, Y.K. Kim, W. Choi, J. Phys. Chem. C 115 (2011) 6141–6148.
[18] T.H. Jeon, W. Choi, H. Park, J. Phys. Chem. C 115 (2011) 7134–7142.
[19] R.M. Cornell, U. Schwertmann, The Iron Oxides: Structure, Properties, Reactions, Occurrences and Uses, 2nd ed., Wiley-VCH, Weinheim, 2003.
[20] U. Bjorksten, J. Moser, M. Gratzel, Chem. Mater. 6 (1994) 858–863.
[21] P.H. Borse, H. Jun, S.H. Choi, S.J. Hong, J.S. Lee, Appl. Phys. Lett. 93 (2008) 173103–173105.
[22] I. Cesar, A. Kay, J.A.G. Martinez, M. Gratzel, J. Am. Chem. Soc. 128 (2006) 4582–4583.
[23] M.P. Dareedwards, J.B. Goodenough, A. Hamnett, P.R. Trevellick, J. Chem. Soc.-Faraday Trans. I 79 (1983) 2027–2041.
[24] J.H. Kennedy, K.W. Frese, J. Electrochem. Soc. 125 (1978) 709–714.
[25] J.H. Kennedy, K.W. Frese, J. Electrochem. Soc. 125 (1978) 723–726.
[26] R. Schrebler, K. Bello, F. Vera, P. Cury, E. Munoz, R. del Rio, H.G. Meier, R. Cordova, E.A. Dalchiele, Electrochem. Solid State Lett. 9 (2006) C110–C113.
[27] F.L. Souza, K.P. Lopes, E. Longo, E.R. Leite, Phys. Chem. Chem. Phys. 11 (2009) 1215–1219.
[28] Y. Hida, H. Kozuka, Thin Solid Films 476 (2005) 264–271.
[29] J.S. Jang, K.Y. Yoon, X.Y. Xiao, F.R.F. Fan, A.J. Bard, Chem. Mater. 21 (2009) 4803–4810.
[30] S.D. Tilley, M. Cornuz, K. Sivula, M. Gratzel, Angew. Chem. Int. Ed. 49 (2010) 6405–6408.
[31] D.K. Zhong, J.W. Sun, H. Inumaru, D.R. Gamelin, J. Am. Chem. Soc. 131 (2009) 6086–6087.
[32] V.M. Aroutiounian, V.M. Arakelyan, G.E. Shahnazaryan, H.R. Hovhannisyan, H.L. Wang, J.A. Turner, Solar Energy 81 (2007) 1369–1376.
[33] S. Saremi-Yarahmadi, K.G.U. Wijayantha, A.A. Tahir, B. Vaidhyanathan, J. Phys. Chem. C 113 (2009) 4768–4778.
[34] Y.S. Hu, A. Kleiman-Shwarsctein, G.D. Stucky, E.W. McFarland, Chem. Commun. 265 (2009) 2–2654.
[35] T. Droubay, K.M. Rosso, S.M. Heald, D.E. McCready, C.M. Wang, S.A. Chambers, Phys. Rev. B 75 (2007) 104412–104418.
[36] J. Velev, A. Bandyopadhyay, W.H. Butler, S. Sarker, Phys. Rev. B 71 (2005) 205208–205214.
[37] F.J. Morin, Phys. Rev. 83 (1951) 1005–1010.
[38] J.S. Jang, J. Lee, H. Ye, F.R.F. Fan, A.J. Bard, J. Phys. Chem. C 113 (2009) 6719–6724.
[39] A. Kleiman-Shwarsctein, M.N. Huda, A. Walsh, Y.F. Yan, G.D. Stucky, Y.S. Hu, M.M. Al-Jassim, E.W. McFarland, Chem. Mater. 22 (2010) 510–517.
[40] A. Kleiman-Shwarsctein, Y.S. Hu, A.J. Forman, G.D. Stucky, E.W. McFarland, J. Phys. Chem. C 112 (2008) 15900–15907.
[41] H. Yong-Sheng, A. Kleiman-Shwarsctein, A.J. Forman, D. Hazen, J.-N. Park, E.W. McFarland, Chem. Mater. 20 (2008) 3803–3805.
[42] V.M. Aroutiounian, V.M. Arakelyan, G.E. Shahnazaryan, G.M. Stepanyan, J.A. Turner, O. Khaselev, Int. J. Hydrogen Energy 27 (2002) 33–38.

[43] V.M. Aroutiounian, V.M. Arakelyan, G.E. Shahnazaryan, G.M. Stepanyan, E.A. Khachaturyan, H. Wang, J.A. Turner, Solar Energy 80 (2006) 1098–1111.
[44] M.N. Huda, A. Walsh, Y. Yan, S.-H. Wei, M.M. Al-Jassim, J. Appl. Phys. 107 (2010) 123712.
[45] Y.S. Hu, A. Kleiman-Shwarsctein, A.J. Forman, D. Hazen, J.N. Park, E.W. McFarland, Chem. Mater. 20 (2008) 3803–3805.
[46] F. Miao, Z. Deng, X. Lv, G. Gu, S. Wan, X. Fang, Q. Zhang, S. Yin, Solid State Commun. 150 (2010) 2036–2039.
[47] M.A. Mousa, A.M. Summan, M.A. Ahmed, A.M. Badawy, J. Mater. Sci. 24 (1989) 2478–2482.
[48] N. Guskos, G.J. Papadopoulos, V. Likodimos, S. Patapis, D. Yarmis, A. Przepiera, K. Przepiera, J. Majszczyk, J. Typek, M. Wabia, K. Aidinis, Z. Drazek, Mater. Res. Bull. 37 (2002) 1051–1061.
[49] S. Krehula, S. Music, J. Alloys Compd. 431 (2007) 56–64.
[50] R.L. Spray, K.S. Choi, Chem. Mater. 21 (2009) 3701–3709.
[51] H. Park, W. Choi, M.R. Hoffmann, J. Mater. Chem. 18 (2008) 2379–2385.
[52] Y.K. Kim, H. Park, Energy Environ. Sci. 4 (2011) 685–694.
[53] D.R. Lide, CRC Handbook of Chemistry and Physics, vol. 90, CRC Press, New York, 2009.
[54] T.-H. Fang, W.-J. Chang, Appl. Surf. Sci. 252 (2005) 1863–1869.
[55] W.H. Strehlow, E.L. Cook, J. Phys. Chem. Ref. Data 2 (1973) 163–199.
[56] S. Trasatti (Ed.), Electrodes of Conductive Metallic Anodes, New York, 1980.
[57] L. Pan, M. Xu, Z.D. Zhang, Mater. Chem. Phys. 123 (2010) 293–299.
[58] K. Kinoshita, Electrochemical Oxygen Technology, John Wiley & Sons, New York, 1992.
[59] R.L. Spray, K.J. McDonald, K.S. Choi, J. Phys. Chem. C (2011), dx.doi.org/10.1021/jp1093433.
[60] F.L. Formal, N. Tetreault, M. Cornuz, T. Moehl, M. Gratzel, K. Sivula, Chem. Sci. 1030 (2001), doi:10.1039/cc00578a.
[61] H.O. Finklea (Ed.), Semiconductor Electrodes, Elsevier, New York, 1988.
[62] J.A. Glasscock, P.R.F. Barnes, I.C. Plumb, N. Savvides, J. Phys. Chem. C 111 (2007) 16477–16488.
[63] E. Thimsen, S. Biswas, C.S. Lo, P. Biswas, J. Phys. Chem. C 113 (2009) 2014–2021.